Lab on a Chip

Accepted Manuscript

ROYAL SOCIETY OF CHEMISTRY

www.rsc.org/loc

Journal Name

ARTICLE

Monitoring of Chromosome Dynamics of Single Yeast Cell in a Microfluidic Platform with Aperture Cell Traps

Received 00th January 20xx,
Accepted 00th January 20xx

DOI: 10.1039/x0xx00000x

www.rsc.org/

Si Hyung Jin,[a] Sung-Chan Jang,[a] Byungjin Lee,[a] Heon-Ho Jeong,[a] Seong-Geun Jeong,[a] Sung Sik Lee,*[b, c] Keun Pil Kim[d] and Chang-Soo Lee*[a]

Chromosome movement plays important roles in DNA replication, repair, genetic recombination, and epigenetic phenomena during mitosis and meiosis. In particular, chromosome movement in the nuclear space is essential for the reorganization of the nucleus. However, conventional methods to analyze the chromosome movements in-vivo have been limited by technical constraints of cell trapping, cell cultivation, oxygenation, and in situ imaging. Here, we present simple microfluidic platform with aperture-based cell trapping arrays to monitor the chromosome dynamics in single living cells for a desired period. Under the optimized condition, our microfluidic platform shows a 57% of single cell trapping efficiency. This microfluidic approach enables in-situ imaging of intracellular dynamics in living cells responding to variable input stimuli under the well-controlled microenvironment. As a validation of this microfluidic platform, we investigate fundamental features of dynamic cellular response of individual cells treated with different stimuli and drug. We prove the basis for dynamic chromosome movement in single yeast to be telomere and nuclear envelope ensembles that attach to and move in concert with nuclear actin cables. Therefore, these results illustrate the capacity to monitor cellular functions and obtain dynamic information at high spatiotemporal resolution through the integration of a simple microfluidic platform.

Introduction

Chromosome movement plays an important role in chromosomal processes during the cell cycle.[1] Organized chromosomes congregate and segregate at mitosis, and active movement of chromosome also occurs during DNA replication, DNA repair, epigenetic regulation, and meiotic recombination. In particular, chromosome movement is significant during meiosis ("prophase I") because homologous maternal and paternal chromosome have to recognize each other or a chromosome pair efficiently.[1,2] In meiotic cells, heterogeneity of dynamic chromosome movements is frequently identified. Thus, there exists a growing interest to track chromosome dynamics of meiotic cells at the single cell level.

Budding yeast is a widely used eukaryotic model organism to study chromosome dynamics due to its simple morphology, well-defined cell cycle, and facile genetics.[1-5] We can identify gene's function and role by simply disrupting, deleting, or inserting genes.[4-10] Several budding yeast mutants exhibit aberrant chromosome dynamics.[3,4] Fluorescent proteins (FPs) are used to label chromosomal and nuclear proteins and specific chromosomal regions allowing to track dynamic chromosomal organization during yeast cell cycles.[10-13] However, it is still difficult to image and track *in vivo* chromosome dynamics in single cells due to cellular movement, oxygen limitation, and the uneven imaging focal plane even with specific control of a microenvironment.

In order to monitor the dynamics of chromosomes, budding yeast cells are conventionally immobilized into low melting (37 °C) agarose gel containing the appropriate medium.[12,14,15] This conventional method of hydrogel based-immobilization can be elaborate, limits initial time-point access during imaging time course experiments, and poses a barrier to rapid and efficient chemical microenvironment control of individual cells. While in other fields progress in assessing cellular response and dynamics derives from improvements in microscopic imaging technique, including microenvironment controls to permit cell growth during extended monitoring time and auto-focusing system enhanced imaging quality, the detailed understanding of chromosome movement has been slowed by the inadequate cell immobilization methodology.

Currently, high-resolution light microscopy depends on dedicated imaging instrumentation and is generally restricted to serial analysis.[16,17] Recent progress of robotics, microfabrication, and miniaturization technology has facilitated the investigation of cellular responses to many stimuli in serial and parallel mode.[18-20] In particular,

[a] Department of Chemical Engineering, Chungnam National University, 99 Daehak-ro, Yuseong-Gu, Daejeon, 305-764, Republic of Korea. E-mail: rhadum@cnu.ac.kr
[b] Institute of Biochemistry, ETH Zürich, Zürich, CH 8093, Switzerland. E-mail: leesu@ethz.ch
[c] Scientific Center for Optical and Electron Microscopy (ScopeM), ETH Zürich, Zürich, CH-8093, Switzerland.
[d] Department of Life Science, Chung-Ang University, Seoul, 156-756, Republic of Korea.
‡ Electronic Supplementary Information (ESI) available: Fig. S1 and Movie S1 to S4. See DOI: 10.1039/x0xx00000x

microfluidic approaches have been developed for the culture of a wide range of cell types.[22-26] However, prevailing application of these microfluidic devices has been limited due to critical technical issues such as complex microfabrication, elegant operation of multilayer micro-valve devices, integration with high-resolution imaging and automation system, and difficulties in microfluidic design with multi-purpose.

Here, we present a microfluidic platform for live cell imaging with capacity for high-resolution imaging technique in space and time. The design of the microfluidic platform embodies a balance among long-term monitoring of living cells or cultivation, the analysis of dynamic cellular response in single cell level, imaging resolution, experimental convenience, and simplicity for easy implementation. The microfluidic platform can accommodate optical objectives with high magnification and numerical aperture (N.A.) for high resolution imaging of cellular response. This microfluidic platform with a cell trap array of horizontal aperture efficiently immobilizes yeast cells, enables us to image high spatial resolution of single cells, and analyze chromosome dynamics in single meiotic yeast cells. Also, after trapping cells, we easily induce meiosis by providing sporulation medium at a specific time, disrupt actin cables by Latrunculin B treatment, and continuously monitor the dynamics of target proteins at single cell level. In this study, we obtain key measurements of yeast cell response in the microfluidic platform, revealing that pachytene chromosome motion requires both actin and telomere/nuclear envelop (NE) association. These data, consistent with conventional methodological results, demonstrate the benefit of a simple microfluidic platform in which high resolution time-lapse microscopic imaging can be performed under an array of experimental conditions and with longer monitoring time.

Experimental

Yeast strains and liquid mediums

The yeast strains used in this study were isogenic heterothallic SK1 derivatives. Cell image analysis utilized the following strains: *lys2::tetO x 240::URA3/+, leu2::LEU2-TetR-GFP* (KKY619); *ZIP1-GFP (700)* (KKY1319); *NUP49-GFP::URA3* (KKY623). All yeast strains were selected in YPG medium (1% w/v yeast extract, 2% w/v bactopeptone, 2% w/v glycerol) at 30 °C for 16 hr. Cells were then inoculated into YPD medium (1% w/v yeast extract, 2% w/v bactopeptone, 2% w/v glucose) at 30℃. After overnight incubation, 4 µl of cell suspension were re-suspended in 4 ml of fresh YPD medium and sub-cultured at 30 °C, 6 hour. Before loading cell suspension into microfluidic device, the cell suspensions were diluted fresh YPD medium until the cell suspension measured OD_{600} to 0.1. Sporulation media (SPM, 1% w/v potassium acetate, 0.02% raffinose) and Latrunculin B (LatB) were purchased from Sigma-Aldrich (MO, USA).

Microfluidic device fabrication

We fabricated the microfluidic devices by soft lithography with microfabricated wafers and poly(dimethylsiloxane) (PDMS, Sylgard 184, Dow Corning, MI, USA). The wafer molds were fabricated by using a negative photoresist (SU-8 3005, MicroChem, MA, USA). Uncured PDMS mixture (10:1 mixing ratio of elastomer and cross-linker) was poured onto the wafer mold to obtain a 5 mm thick layer and then fully cured at 65 °C for 4 hour. It was later peeled off from the wafer mold and individual devices were cut to size. Holes for fluidic connections were introduced with 0.75 mm diameter biopsy tools. PDMS devices were plasma bonded onto a cover glass (150 µm) for high-resolution imaging.

Image analysis

Yeast cells and GFP signals were imaged with a Nikon TE 2000U inverted fluorescence microscope with a 100x oil-immersion objective (*N.A.* = 1.45), and FITC filter sets. Image analysis was performed with Image-pro (Media Cybernetics, MD, USA) and ImageJ software. The 3D shapes of chromosomes were imaged with a Nikon A1 confocal microscope with a 100x oil-immersion objective (*N.A.* =1.45). Image analysis was performed with the NIS-Elements (Nikon, Japan) and the reconstructed image was acquired using the Imaris (Bitplane, MA, USA) image software.

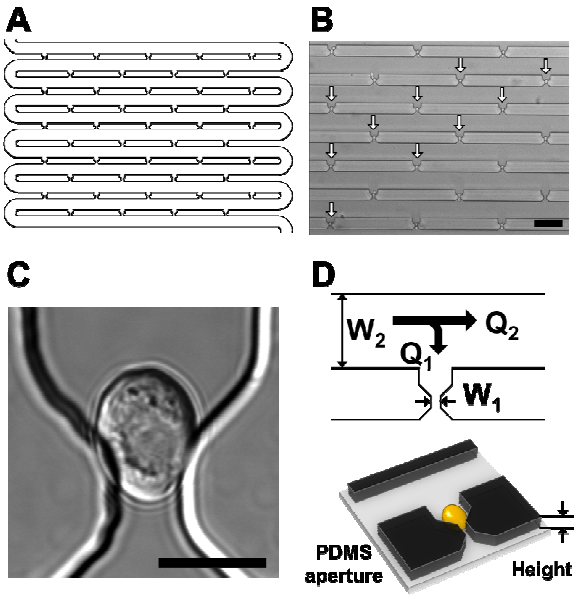

Fig. 1 Microfluidic platform for single cell trapping and tracking of cell dynamics. (A) Each microfluidic aperture trap array consists of wide main cell-delivery channel arranged in a 10-column format and an array of cross-flow channels that connect each section of the main channel. (B) Bright-field image showing an array of aperture trap filled with single cells that are identified by white arrows (trap width; W_1 = 3 µm). Scale bar indicates 50 µm. It shows efficient trapping capacity of single-cell in the array (57 %). White dots indicate single cell trapping. (C) Enlarged image of single yeast cell trapped (Scale bar = 5 um). (D) Schematic drawing of the trajectory of flow, indicating important variables influencing trapping efficiency.

Results and discussion

Fig. 1 illustrates basic design of single-layer microfluidic platform for high-resolution time-lapsed imaging with inexpensive, disposable, easy fabrication, simple operation and expandable multiplexing capacity of cell culture and analysis. The microfluidic device consists of a wide serpentine-like main delivery channel and several cell traps located vertically (Fig. 1A). The cell trap array has parallel apertures whose dimension fit the size of yeast, with the width of a single aperture (W_1 = 3 μm) smaller than the average size of yeast cell (5 μm) allowing capture along the main channel (Fig.1B and C). Images of the fabricated microfluidic channel filled with yeast cell are shown in Fig. 1B and C.

The basic principle of the cell trapping is depicted in Fig. 1D and is similar to that of a sieve.[26-31] Simply, cells smaller than the trap gap size (W_1) pass through the trap, whereas cells larger than the gap size are trapped geometrically. In addition, we use the fluidic pressure difference as a driving force for trapping cells. Specifically, while yeast cells pass through a main delivery channel, cells near an aperture trap are drifted into two streams: the main stream (Q_2) flowing along the main delivery channel and a second stream (Q_1) that directs a cell into the trap. Cell trapping is similar to the cellular valving method based on a differential fluidic resistance of two streams which is adopted from the serpentine microfluidic arraying system.[27-31] The process enables the serial arraying of cells while the cells are trapped, acting as a valve in the open state. In this manner we successfully form array of more than 95 single living cells in a single microchannel.

The dimensions of the microfluidic aperture and optimum flow rate for efficient cell trapping were optimized. We varied the height of the aperture (H) from 6 to 11 μm, whereas the width of W_1 and W_2 were fixed at 3 and 30 μm, respectively (Fig. 2A). The number of trapped cells was highly related to the dimension of the microfluidic aperture. Higher height allowed more available space for cell occupancy. The effect of dimension of the microfluidic aperture on trapping was investigated with 6, 8, and 11 μm height with a flow rate at 1 μl min^{-1}. In microfluidic device with 6 μm height, the Q_1/Q_2 value is equal to 1.42 and 59% of the stream flows toward the aperture cell trap. At 11 μm height, the Q_1/Q_2 value is equal to 0.58, and only 37% of the stream flows toward the aperture cell trap. Following these ratios, different percentage values for cell trapping were obtained at each height of the microfluidic aperture. All results were generated from average values of five data series measured in five tested devices under the same experimental conditions. Fig. 2A shows that 6 μm

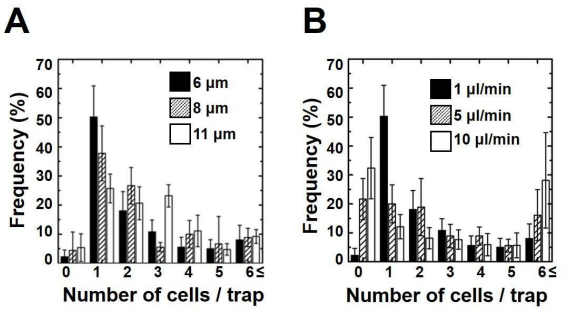

Fig. 2 Experimental result of cell trapping in the microfluidic aperture with various heights and flow rates. Each bar represents the percentage of microfluidic aperture occupied by zero, one, two, three, four, five, and above six cells. (A) The different height of the main channel (H) varied from 6 to 11 μm on the frequency of cell trapping while the width of main channel (W_2) and trap (W_1) are fixed at 30 μm and 5 μm, respectively. The percentage of the microfluidic aperture containing zero, one, two, three, four, five, and above six cells is shown in accordance with different heights of the microfluidic aperture at constant flow rate (1 μl min^{-1}). (B) The effect of flow rate on the number of cells trapped at 6 μm height of the microfluidic aperture. The error bars in both (A) and (B) indicate the standard deviations.

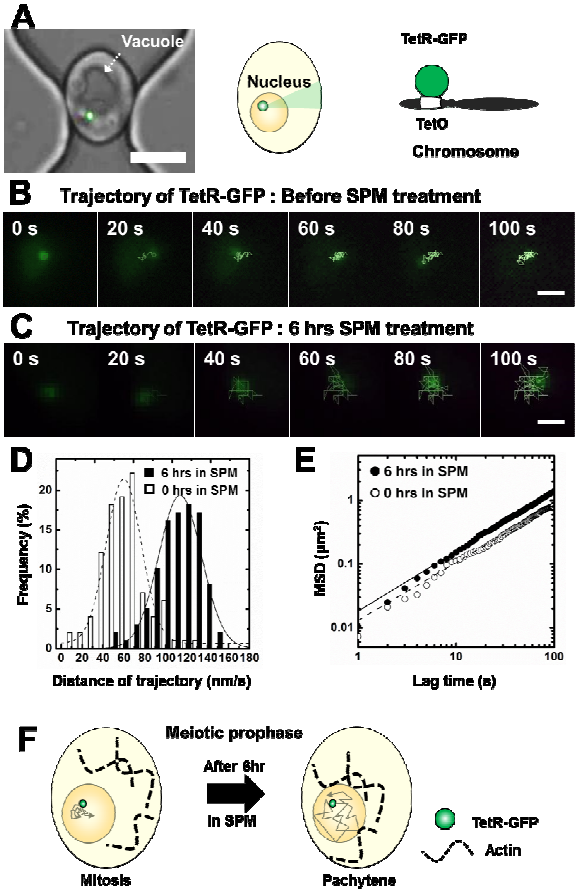

Fig. 3 Chromosome movement with TetR-GFP. (A) Model of chromosome movement; schematic diagram of visualization of chromosome expressing TetR-GFP that carries GFP-labeled *tetO* repeats. Enlarged optical image of single yeast trapped. The scale bar represents 2 μm. (B) Time-lapse fluorescent microscopic images (20 second intervals) of single live cells undergoing chromosome movement with monitoring displacement of TetR-GFP before treatment of sporulation medium (SPM). We monitor movement of TetR-GFP and evaluated the trajectory of TetR-GFP in a single cell. (C) Movement of TetR-GFP after 6 hours incubating in SPM medium. The treatment of SPM makes the cell pachytene stage. Scale bar indicates 2 μm. (D) Histogram of the distances of TetR-GFP movement per second before and after treatment of SPM medium for 6 hours, respectively. (E) Mean square displacement (MSD) of chromosome movement with TetR-GFP before and after 6 hrs of SPM treatment. (F) Schematic diagram of TetR-GFP movement in each cell stage of meiosis.

height of the microfluidic aperture enabled efficient single cell trapping. The height increase of the microfluidic aperture increased the number of cells trapped. The flow rate is another important variable parameter for cell trapping (Fig. 2B). The microfluidic device strongly depended on fluidic pressure difference as the main driving force for trapping into the microfluidic aperture. Hence, if the velocity of the bulk flow (Q_2) was increased, cells easily drifted the microfluidic aperture due to the decrease of trapping flow (Q_1). In single cell trapping, low flow rate (1 µl min^{-1}) showed 50% efficiency and the increase of flow rate dramatically decrease single cell trapping efficiency.

The geometric confinement of the aperture cell trap is another important technical issue that can affect the life of budding yeast. Diploid budding yeast initiates meiosis under starvation conditions, but sufficient aeration and nutrients and the appropriate acidity (pH) are necessary for efficient meiosis and chromosome movement. If traps are too tight, budding yeast will not progress efficiently through the meiotic cell cycle due to oxygen limitations and pH changes. Under optimized conditions, we analyzed the growth rate of yeast cells in our aperture cell trap to investigate the effects of geometric confinement on cell growth. The results clearly confirm that our aperture cell trap did not influence yeast growth (Fig. S1A, ESI‡). The measured doubling time of the KKY 619 strain in the aperture cell traps was approximately 2 hours 40 min. In comparison, the growth curve analysis performed with identical strains and measured using a UV spectrometer indicated that the doubling time was approximately 2 hours 44 min (Fig. S1B, ESI‡). These experimental results imply identical cell viabilities between the aperture cell trap and conventional flask culture. Thus, it is reasonable to conclude that the aperture cell trap with geometric confinement provides favorable cell culture conditions.

We perform an on-chip viability study of budding yeast to determine whether trapping and given-perfusion flow induce cell damage during budding and division (Fig. S1 and 2, ESI‡). The platform of the microfluidic device allowed imaging of budding initiation (arrow in Fig. S2B, 3 hour) and mitotic cell division while continuously providing cell culture media (Yeast extract Peptone Dextrose (YPD)) during 6 hours (Fig. S2A and B, ESI‡). Budding yeast divide asymmetrically in nutrient rich medium, while nutrient limitation induces meiosis and sporulation. Thus, meiosis is induced by switching the cell culture media to sporulation media (SPM) lacking glucose and nitrogen source. As expected, budding yeast cells in microfluidic aperture traps are first exposed to sporulation medium to initiate meiosis and observe the typical morphology of meiosis that forms four daughter cells (Fig. S2C and D, ESI‡). Together our results indicate that the microfluidic device is suitable for the investigating yeast cell biology over a range of cell stages, and that we can monitor individual cells undergoing the developmental transition from mitosis phase to meiosis at the single cell level.

To examine a capability of the microfluidic device for the analysis of cellular events at a single cell level, we investigated chromosome dynamics of yeast in meiosis by precise quantification of chromosome movement using the microfluidic device to enable cell trapping and *in-situ* cell imaging with relatively high resolution (oil immersion objective lens, *N.A.*=1.45). When GFP-repressor fusions bind to operator arrays, they produce a bright dot that can be followed in live cells by time-lapse monitoring of fluorescent signal. In this study, we used diploid yeast strain carrying GFP-labeled Tet-operator (*tetO*) repeats to visualize chromosomes as single bright dots in the cell (Fig. 3A). Cells expressed protein tagged with green fluorescent protein (GFP), TetR-GFP, serving as a visual marker for chromosome movement because a small fluorescent dot is present on chromosomes at the positions of the *tetO* arrays.

Sequential images were able to quantify chromosome movement by measuring the total distance of the bright fluorescence dot's trajectory during an imaging time series (Fig. 3B and 3C). We compare dynamic chromosome behavior of mitotic (before treatment of SPM) and meiotic chromosomes (after 6 hour treatment of SPM medium) (Fig. 3D). In yeast, the zygotene and pachytene stages occur

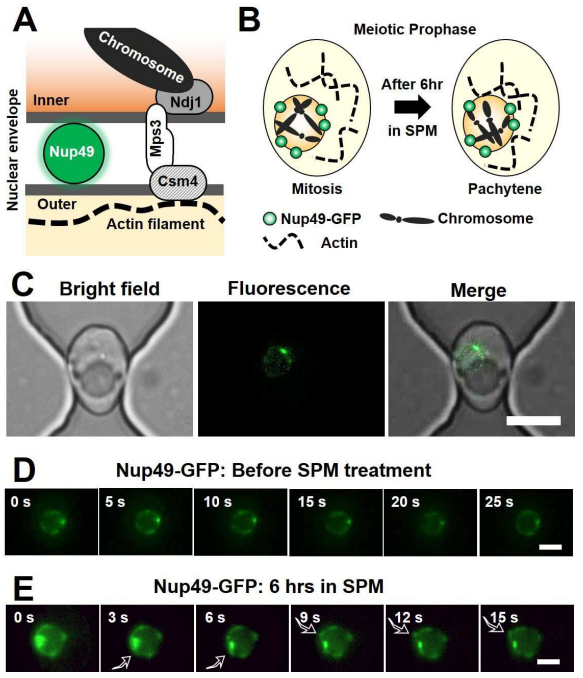

Fig. 4 Movement of nuclear envelope at pachytene state. (A) Schematic diagram of telomere-led chromosome and nuclear envelope (NE): In this study, nuclear pore component labeled with GFP (Nup49-GFP) is utilized for visualization. Mono-Polar Spindle 3 (Mps3); Non-DisJunction 1 (Ndj1); Chromosome Segregation in Meiosis 4 (Csm4). (B) Schematic representation of the dynamics of nuclear envelope: the attachment of actin would be associated in meiosis phase. (C) Representative images of Nup49-GFP in singe cell that trapped in microfluidic device (Bright field, Fluorescence, and Merged image). Scale bar indicates 5 µm. (D) 2D time-lapse images of pachytene nuclei with Nup49-GFP labeled NE, captured at 5 second intervals before SPM medium treatment. Scale bar indicates 2 µm. (E) 2D time-lapse images of pachytene nuclei with Nup49-GFP labeled NE, captured at 3 second intervals after incubated in the SPM medium for 6 hour. Arrows indicate angular deformation. The movement of Nup49-GFP becomes more active at pachytene, with long protrusions limited to the period. Scale bar indicates 2 µm. (See the Movie S3, ESI‡)

sequentially. Chromosome movement exhibits the same progression. Chromosome dynamics were independently examined by monitoring of TetR-GFP movement (Fig. 3B and 3C). Analysis of TetR-GFP trajectories reveals that mobility is changed from mitotic chromosome (t = 0; before SPM treatment) through meiotic chromosome (t = 6 hour) and is even more dramatic at pachytene (t = 6 hour) (Fig. 3B to 3C, S3A in ESI‡). The movement of chromosome initiates prophase although beginning of zygotene is tightly linked to a key step of meiotic recombination. In meiosis, onset of motion may be part of the basic cellular program that becomes coupled to progression of recombinational progression by coordinating regulatory mechanisms.[4] Statistically, the average movement of GFP dot obtained from 45 individual cells were tracked and analyzed (Fig. 3D and S3A, ESI‡). Trajectory analysis of chromosomes in live cells showed that chromosome movement is relatively slow before treatment of SPM while average chromosome movement is induced in the SPM medium. As a result, following incubation in the SPM medium for 6 hours, pachytene chromosomes showed more movement than either the mitotic chromosome or the zygotene chromosome (Fig. 3D and S3A, Movie S1‡ and 2‡). We quantitatively analyzed the movement of the tracking label in single cells by mean square displacement (MSD) and its trend in accordance with the observed lag time from the first analyzed time-point in the trajectory analysis (Fig. 3E). The correlation between lag time and the MSD of a particle in 2 dimensions can be calculated using equation (1).

$$MSD = 4D\tau^{\alpha} \quad (1)$$

where, D indicates the diffusivity and τ stands for the observed lag time. Generally, the exponent α distinguishes the type of diffusion that particles encountered: α = 1, normal Brownian diffusion in purely viscous (liquid-like) material, e.g. water; α < 1, sub-diffusion in elastic material; and α > 1, super-diffusion or active movement. The results clearly indicate that the labels moved sub-diffusively, which may be due to the crowding of the nucleus (exponents for α were 0.9598 and 0.989 before treatment and after 6 hours of treatment with SPM, respectively) and the elastic property of the cytosolic fluid, which contains several biomaterials (i.e., DNA, proteins, carbohydrates, lipids, etc.). More interestingly, the diffusivity of the label increased when we treated with SPM medium over 6 hours (the diffusivity equaled 2.67 x 10^{-3} and 3.77 x 10^{-3} μm^2 s^{-1}, before and after 6 hours of treatment with SPM, respectively). This result implies that actin filaments contribute to the movement associated with the nuclear envelope in the pachytene stage, as illustrated in Fig. 3F and Fig. 4A and B. We believe that the results presented here shed very original perspectives on the potential interplay between the chromosome/chromatin physical status and the biological events processed at the same time under controlled conditions. Taken together, accurate and precise quantification of chromosomal dynamics indicates that the movement of meiotic chromosomes is particularly significant at the pachytene state (Fig. 3F). All of the results provide clear evidence in budding yeast that nutrients strongly affect rapid chromosome movements. Taken together, our microfluidic approach enables analysis of chromosome dynamics by simple monitoring of GFP-tagged chromosomes in which arrays of *Tet*-operator sites are integrated into defined sites in the genome followed by TetR-GFP expressed. On the basis of these observations, we can confirm that during meiotic prophase the presence of rapidly moving chromosomes over an extended period of time.

Next, we focus on chromosome dynamics associated with the nuclear-envelop (NE) and actin to study the basis of

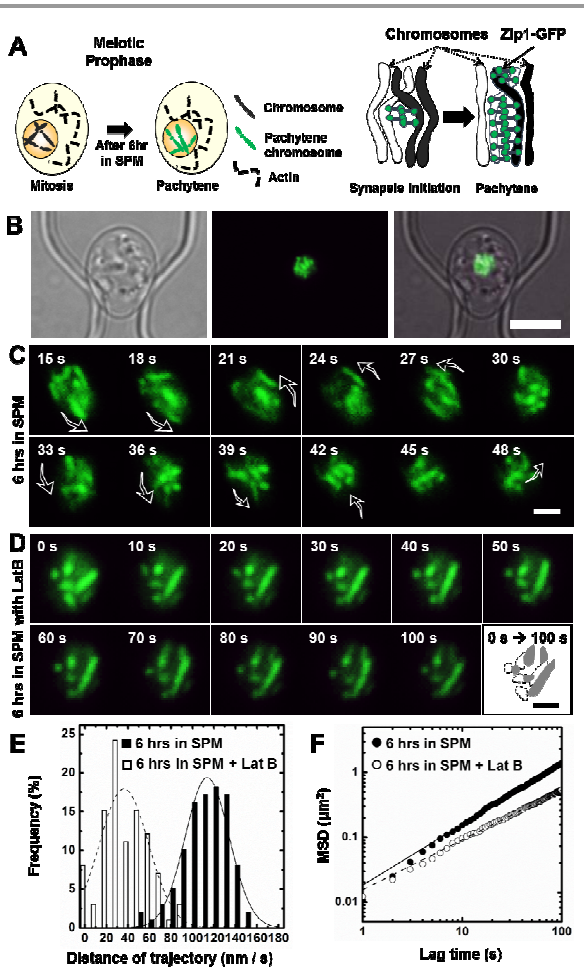

Fig. 5 Actin associated chromosome movement at pachytene state. (A) Schematic diagram of the Zip1-GFP strain. At prophase, *ZIP1* acts as a molecular zipper to bring homologous chromosomes into close apposition. ZIP1 may encode the transverse filaments of the synaptonemal complex. (B) Experimental images of a singe cell trapped in the microfluidic device with expression of Zip1-GFP (Bright field, Fluorescence, and Merged image). Scale bar = 5 μm. 3D reconstruction of pachytene chromosomes obtained from confocal images is available in Movie S4‡. (C) Time-lapsed images of pachytene chromosome with expressing Zip1-GFP (6hr after meiosis induction; 3s intervals) before the treatment of LatB. Arrows indicate discrete and directed motion. See also Movie S5‡. (D) Time-lapsed images of pachytene chromosome with expression of Zip1-GFP after the treatment with 20 μM LatB. The treatment of LatB significantly reduces movement of pachytene chromosome. Scale bar = 2 μm. (E) Frequency of distance of trajectory of TetR-GFP at the pachytene stage without or with treatment of 20 μM LatB. (Movie S6, ESI‡). (F) Mean square displacement (MSD) of chromosome movement with or without 20 μM LatB treatment.

dynamic mid-prophase I (pachytene) telomere-led chromosome motion in budding yeast. Previous studies have implied that individual telomere/nuclear envelope (NE) complexes associate with nucleus-hugging actin cables that are continuous with the global cytoskeletal actin network and move for a few seconds in conjunction with the cables (Fig. 4A and 4B).[1,4] Conformational deformation of NE results in telomere-led chromosome movement because pachytene chromosome ends are robustly associated with the NE.[1,4] With our microfluidic device, we visualize the NE by time-lapse imaging of fluorescently expressed nuclear pore component Nup49-GFP (Fig. 4C). After trapping single cells, confocal fluorescence microscopy image clearly showed the NE. The time-lapse analysis of Nup49-GFP dynamics confirmed that telomere-led chromosome movement is accompanied by concomitant local NE deformation. In vegetative growth and early meiosis, the NE exhibited a static spherical or oval shape. However, at the pachytene chromosome state (at t = 6 hours), NE showed dynamic conformational changes (Fig. 4D and 4E, Movie S3‡). Common local shape changes were angular deformations of NE, in which the deformation evolved into thin and short protrusions or recession (up to 0.3 μm). Dynamic changes of NE shape could also be correlated with directional telomere-led chromosome movement. As shown in the sequence of Fig. 4E, at 0 to 6 second, an angular deformation, likely with a short protrusion, occurred at the leading end of a single chromosome. At a different position on the nucleus (9 to 15 second, Fig. 4E), outward-directed movement accompanied elongation of the surrounding NE segment. This change was followed by movement of the body of the nucleus in the opposite direction. Thus, we conclude that directional force is exerted specifically on telomere/NE ensembles, moving the targeted chromosome end and concomitantly deforming the NE at the affected point.

The process of chromosome pairing and chromosome motility after pairing are of interest because reciprocal recombinations between homologous chromosomes take place during the prophase of first meiotic division and these are essential for proper segregation.[32-34] The consecutive changes that occur to chromosomes during prophase have only begun to be characterized by live imaging techniques at single cell level. Thus, we wanted to investigate the feasibility of the microfluidic device to monitor and analyze sequential changes of chromosome behavior. For the study of the dynamics of synaptonemal complexes (SCs) during prophase of meiosis, a Zip1-GFP (molecular zipper) was applied to visualize SCs in live sporulating yeast cells because *ZIP1* is an integral and essential protein component of the central element of the synaptonemal complexes (SCs)[6] and is believed to be the ortholog of the mammalian protein *SYCP1*.[35] Overall schematic diagram of chromosome pairing with Zip1-GFP imaging is shown in Fig. 5A.

After trapping single cells in the microfluidic device, pachytene chromosomes were clearly observed by confocal fluorescence microscopy (Fig. 5B). At prophase, *ZIP1* acts as a molecular zipper to bring homologous chromosomes into close apposition. *ZIP1* may encode the transverse filaments of the SC (Fig. 5A). Fig. 5B shows that the microfluidic device renders proper condition for sequential imaging of the trapped cells. Also, as expected, we could monitor chromosome motion by imaging Zip1-GFP in the pachytene chromosomes. Dynamic chromosomal movement was monitored with 3 seconds intervals in living cells after incubation for 6 hours in the SPM medium.

To gain further insight into the role of nuclear deformation by actin, we treat the yeast cells with Latrunculin B (LatB). LatB is a disruptor of microfilament organization because it can bind to actin monomers and inhibits actin polymerization *in vitro,* disrupting microfilament organization as well as actin filament-mediated processes during cellular processes.[36] In the absence of LatB, we observe a notable rotation of individual chromosome (SC) (Fig. 5C). However, there was a significant decrease of *in vivo* chromosome motion from cells treated with LatB (Fig. 5D). The treatment of LatB induced chromosome movement to small "jiggling" motions (Fig. 5D). In order to verify the effect of LatB, we quantified chromosome movement in 100 cells by imaging TetR-GFP-labeled *tetO* repeats as we previously show in Fig. 3. Indeed, we found a significant decrease of chromosome movement upon the addition of LatB (Fig. 5E, F and S3B, ESI‡). After 6 hours of treatment with LatB, the exponent α was 0.7946, and the diffusivity was 3.54×10^{-3} $\mu m^2 s^{-1}$. This result confirms that actin, which would be disrupted upon LatB addition, contributes to chromosome movement. Taken together, these results are consistent with telomere-led chromosome movement and provide new information about the mechanics and movement of yeast meiotic chromosomes. The behavior of whole chromosomes at the pachytene stage of meiotic prophase I as characterized *in vivo* indicates that pachytene chromosomes link to the NE and dynamic movement of actin cables displaces the attached complex. Further, this movement is critical for meiotic recombination biochemistry and chromosome metabolism, and that it is critical for processes by which homologous sequences find each other, joint molecules are made, and homologs become tightly paired in SC.

Conclusions

In conclusion, we monitored chromosome dynamic movements in single living cells for a defined period *via* a simple microfluidic platform with aperture-based cell trapping arrays. Main advantage is high accuracy of measurement for a biological event at the single cell level, because each single cell is physically trapped and cannot migrate or move out of the plane of focus. Our microfluidic platform allows easy and efficient single cell loading while maintaining captured cells in a low shear stress environment for long-term studies. We can investigate the dynamic responses of individual cells treated with different stimuli including physical environment and chemicals.

As a proof-of-principle, we demonstrate the tracking and quantification of chromosome dynamics in yeast cell. Our approach can provide new biological information gained from

single-cell level and *in situ* dynamic response and new opportunities to quantify individual cellular responses as opposed to the averaged information provided by conventional methods. We envision this simple microfluidic approach in tracking chromosome movements will be useful to investigate other cell biological processes requiring single cell feature tracking and quantification, since our approach is not only an ideal imaging platform but also has simplicity of design, inexpensive materials, affordable experimental setup and adaptability for high-throughput assays.

Acknowledgements

We thank the M. Peter lab (ETH Zürich) for ongoing support. We are grateful to Dr. Alicia Smith for helpful comments on this manuscript. This research was supported by the Basic Science Research Program (NRF-2011-0017322 and 2013-020972) and Global Research Laboratory (NRF-2015K1A1A2033054) through the National Research Foundation of Korea (NRF) funded by the Ministry of Science, ICT (Information and Communication Technologies) and Future Planning.

References

1 R. Koszul and N. Kleckner, *Trends Cell Biol.*, 2009, **19**, 716.
2 R. I. Kumaran, R. Thakar and D. L. Spector, *Cell*, 2008, **132**, 929.
3 J. Mine-Hattab and R. Rothstein, *Nat. Cell Biol.*, 2012, **14**, 510.
4 R. Koszul, K. P. Kim, M. Prentiss, N. Kleckner and S. Kameoka, *Cell*, 2008, **133**, 1188.
5 K. P. Kim, B. M. Weiner, L. Zhang, A. Jordan, J. Dekker, and N. Kleckner, *Cell*, 2010, **143**, 924.
6 M. Sym, J. Engebrecht and G. S. Roeder, *Cell*, 1993, **72**, 365.
7 S. Hong and K. P. Kim, *Mol. Cells*, 2013, **36**, 446.
8 H. J. Cha and Y. J. Yoo, *Korean J. Chem. Eng.*, 1996, **13**, 172.
9 H. C. Lee and C. Y. Choi, *Korean J. Chem. Eng.*, 1987, **4**, 47.
10 P. Heun, T. Laroche, K. Shimada, P. Furrer and S. M. Gasser, *Science*, 2001, **294**, 2181.
11 P. Li, H. Jin, M. L. Hoang and H. G. Yu, *Chromosome Res.*, 2011, **19**, 1013.
12 H. Hajjoul, J. Mathon, H. Ranchon, I. Goiffon, J. Mozziconacci, B. Albert, P. Carrivain, J. M. Victor, O. Gadal, K. Bystricky and A. Bancaud, *Genome Res.*, 2013, **23**, 1829.
13 A. Belmont, *Trends Cell Biol.*, 2001, **11**, 250.
14 K. K. Steffen, B. K. Kennedy and M. Kaeberlein, *J. Vis. Exp.*, 2009, DOI: 10.3791/1209.
15 R. K. Mortimer and J. R. Johnston, *Nature*, 1959, **183**, 1751.
16 N. Rosenfeld, J. W. Young, U. Alon, P. S. Swain and M. B. Elowitz, *Science*, 2005, **307**, 1962.
17 J. M. Pedraza and A. van Oudenaarden, *Science*, 2005, **307**, 1965.
18 A. Roguev, M. Wiren, J. S. Weissman and N. J. Krogan, *Nat. Methods*, 2007, **4**, 861.
19 A. H. Y. Tong, G. Lesage, G. D. Bader, H. M. Ding, H. Xu, X. F. Xin, J. Young, G. F. Berriz, R. L. Brost, M. Chang, Y. Q. Chen, X. Cheng, G. Chua, H. Friesen, D. S. Goldberg, J. Haynes, C. Humphries, G. He, S. Hussein, L. Z. Ke, N. Krogan, Z. J. Li, J. N. Levinson, H. Lu, P. Menard, C. Munyana, A. B. Parsons, O. Ryan, R. Tonikian, T. Roberts, A. M. Sdicu, J. Shapiro, B. Sheikh, B. Suter, S. L. Wong, L. V. Zhang, H. W. Zhu, C. G. Burd, S. Munro, C. Sander, J. Rine, J. Greenblatt, M. Peter, A. Bretscher, G. Bell, F. P. Roth, G. W. Brown, B. Andrews, H. Bussey and C. Boone, *Science*, 2004, **303**, 808.
20 S. Cookson, N. Ostroff, W. L. Pang, D. Volfson and J. Hasty, *Mol. Syst. Biol.*, 2005, **1**, 2005 0024.
21 S. S. Lee, I. Avalos Vizcarra, D. H. E. W. Huberts, L. P. Lee and M. Heinemann, *Proc. Natl. Acad. Sci. U. S. A.*, 2012, **109**, 4916.
22 K. Leung, H. Zahn, T. Leaver, K. M. Konwar, N. W. Hanson, A. P. Page, C. C. Lo, P. S. Chain, S. J. Hallam and C. L. Hansen, *Proc. Natl. Acad. Sci. U. S. A.*, 2012, **109**, 7665.
23 Wang, M. C. Kim, M. Marquez and T. Thorsen, *Lab Chip*, 2007, **7**, 740.
24 M. C. Kim, B. C. Isenberg, J. Sutin, A. Meller, J. Y. Wong and C. M. Klapperich, *Lab Chip*, 2011, **11**, 1089.
25 R. J. Taylor, D. Falconnet, A. Niemisto, S. A. Ramsey, S. Prinz, I. Shmulevich, T. Galitski and C. L. Hansen, *Proc. Natl. Acad. Sci. U. S. A.*, 2009, **106**, 3758.
26 H. H. Jeong, S. H. Jin, B. J. Lee, T. Kim and C. S. Lee, *Lab Chip*, 2015, **15**, 889.
27 W. H. Tan and S. Takeuchi, *Proc. Natl. Acad. Sci. U. S. A.*, 2007, **104**, 1146.
28 J. Kim, J. Erath, A. Rodriguez and C. Yang, *Lab Chip*, 2014, **14**, 2480.
29 S. H. Jin, H. H. Jeong, B. Lee, S. S. Lee and C. S. Lee, *Lab Chip*, 2015, **15**, 3677.
30 A. Dewan, J. Kim, R. H. McLean, S. A. Vanapalli and M. N. Karim, *Biotechnol. Bioeng.*, 2012, **109**, 2987.
31 T. Teshima, H. Ishihara, K. Iwai, A. Adachi and S. Takeuchi, *Lab Chip*, 2010, **10**, 2443.
32 S. Tesse, A. Storlazzi, N. Kleckner, S. Gargano and D. Zickler, *Proc. Natl. Acad. Sci. U. S. A.*, 2003, **100**, 12865.
33 S. Hong, Y. Sung, M. Yu, M. Lee, N. Kleckner, and K. P. Kim. *Mol. Cell*, 2013, **51**, 440.
34 S. Tournier, Y. Gachet, V. Buck, J. S. Hyams and J. B. Millar, *Mol. Biol. Cell*, 2004, **15**, 3345.
35 R. L. Meuwissen, H. H. Offenberg, A. J. Dietrich, A. Riesewijk, M. van Iersel and C. Heyting, *EMBO J.*, 1992, **11**, 5091.
36 D. Y. Lui, C. K. Cahoon and S. M. Burgess, *PLoS Genet.*, 2013, **9**, e1003197.